Interference in a quantum dot molecule embedded in a ring interferometer

Thomas Ihn[1,3]**, Martin Sigrist**[1]**, Klaus Ensslin**[1]**,
Werner Wegscheider**[2] **and Matthias Reinwald**[2]

[1] Solid State Physics Laboratory, ETH Zurich, CH-8093 Zurich, Switzerland
[2] Institut für experimentelle und angewandte Physik,
Universität Regensburg, Germany
E-mail: ihn@phys.ethz.ch

Abstract. Interference experiments are presented involving electronic quantum transport through an artificial quantum dot molecule in the Coulomb blockade regime embedded in a ring interferometer. Full tunability and the high stability of the structure allowed the transmission phase through this system, spin-related interference phenomena, and Fano-type interference to be studied. When a part of the interferometer is itself tuned into the Coulomb blockade regime, a phase-coherently coupled triple dot system can be investigated. The experiments demonstrate the feasibility of complex quantum circuits with a high degree of phase-coherence.

[3] Author to whom any correspondence should be addressed.

IOP Institute of Physics **ΦDΦ** DEUTSCHE PHYSIKALISCHE GESELLSCHAFT

Contents

1. Introduction

The quest for new semiconductor devices operating based on quantum mechanical principles requires the realization of well designed phase-coherent quantum circuits with controllable potentials. Phase-coherence of partial waves is a prerequisite for quantum interference, one of the fundamental quantum phenomena. In semiconductor nanostructures, quantum interference of electron waves is found very prominently in the Aharonov–Bohm [1] and the Fano [2] effects. In contrast to photons in vacuum, which do not interact with each other, in the case of electrons the mutual Coulomb interaction between the charged particles can be a significant source of decoherence [3, 4]. Studying interference and decoherence in semiconductor nanostructures is therefore of fundamental interest and of crucial importance for future nanoscale quantum device applications.

After having been observed in metallic nanostructures [5, 6], the Aharonov–Bohm effect was studied in ring-shaped semiconducting devices [7]–[9] coupled to leads via a conductance larger than the quantum conductance $G_0 = e^2/h$. Ring-shaped structures with much weaker coupling to the leads are dominated by interaction effects and exhibit an energy level spectrum periodic in the number of flux quanta $\phi_0 = h/e$ penetrating the ring area [10]. In a novel class of experiments, a quantum dot, i.e., a tailored and well tunable strongly interacting electronic region, was embedded in one interferometer path and partial phase-coherence of the resonant current through the dot could be demonstrated [11]. In the same experiment, the transmission *phase* through the quantum dot measured relative to the reference arm was found to be either 0 or π in agreement with the generalized Onsager relations [12] predicting this so-called 'phase rigidity' for two-terminal devices. In later experiments made to measure the true transmission phase of a quantum dot, the two-terminal geometry was abandoned in favour of multi-terminal configurations [13, 14].

In the simplest fully coherent single-mode picture, the conductance G of a two-terminal device showing the required magnetic field symmetry can be derived from the reflection R via

$$G = 2G_0 \left(1 - R\right), \tag{1}$$

where the factor 2 accounts for spin degeneracy and in lowest order

$$R = \left| r_0 + r_1 e^{i2\pi\phi/\phi_0} + r_1 e^{-i2\pi\phi/\phi_0} + \cdots \right|^2$$

$$= |r_0|^2 + 2|r_1|^2 + 4|r_0||r_1|\cos\delta\,\cos\left(2\pi\frac{\phi}{\phi_0}\right) + \cdots. \tag{2}$$

Here r_0 is the amplitude for direct reflection at the ring entrance and $r_1 = |r_1|\,e^{i\delta}$ is the (complex) amplitude for reflection after travelling once around the ring at zero magnetic field. The magnetic flux $\phi = BA$ with B being the magnetic field (flux density) and A the ring area. The first two terms in equation (2) are relevant for the magnetic field averaged (classical) contribution to the conductance, while the third term describes the Aharonov–Bohm effect, i.e., periodic conductance oscillations with the period of an elementary flux quantum ϕ_0. Although this model is useful and sets the stage for the observation of the Aharonov–Bohm effects in semiconductor nanostructures, it will be shown in this paper that it is of limited use in the interpretation of our experiments.

The Fano effect is due to the interference of a resonant state, such as the discrete level of a quantum dot, and a continuum of states as found in open systems. In semiconductor nanostructures, the Fano effect was first invoked as a speculative explanation of peaked transmission through a quantum point contact [15]. In quantum dots it can occasionally lead to slightly asymmetric line shapes in the case of weak dot–lead coupling [16] and to well pronounced Fano-lineshapes in the case of stronger coupling [17]. Tailored nanostructures for studying the Fano-effect have included a narrow channel with a side-coupled quantum dot [18, 19], an Aharonov–Bohm ring with a side-coupled quantum dot [20] and a series of experiments in which a quantum dot was embedded in one path of a two-terminal Aharonov–Bohm ring [21, 22].

In this paper, we report measurements on a two-terminal ring-shaped geometry in which a quantum dot molecule is embedded such that the two dots sit in the two interference paths and the molecular coupling can be continuously tuned. The sample is similar to that used in [21, 23]. In previous experiments we have studied phase-coherent contributions to the inelastic cotunnelling current through one of the two quantum dots in the case of strong [24] and negligible inter-dot coupling [25]. Here we concentrate on a series of experiments in the linear transport regime showing Aharonov–Bohm and Fano-type interference effects. After the description of our sample and experiment in section 2 and the sample characterization in section 3, we will tie in with the discussion about the transmission phase through a quantum dot raised in [11, 13, 14] in section 4. In section 5, we take up the issue of partial decoherence of the current due to spin-pairing theoretically proposed in [26] and used for the interpretation of the experiments in [22]. In section 6, we show the appearance of the Fano-effect in our sample and in section 7, we present Aharonov–Bohm oscillations in a triple-dot geometry that can be induced in our structure.

2. Sample and experimental set-up

Our sample is built on a Ga[Al]As heterostructure with the heterointerface 34 nm below the sample surface. Close to this interface a two-dimensional electron gas with a sheet electron density $n_s = 5 \times 10^{15}\,\mathrm{m}^{-2}$ and a mobility $\mu = 40\,\mathrm{m}^2\,\mathrm{Vs}^{-1}$ is present at low temperatures as a result of remote doping in the barrier.

**IOP** Institute of Physics **Φ** DEUTSCHE PHYSIKALISCHE GESELLSCHAFT
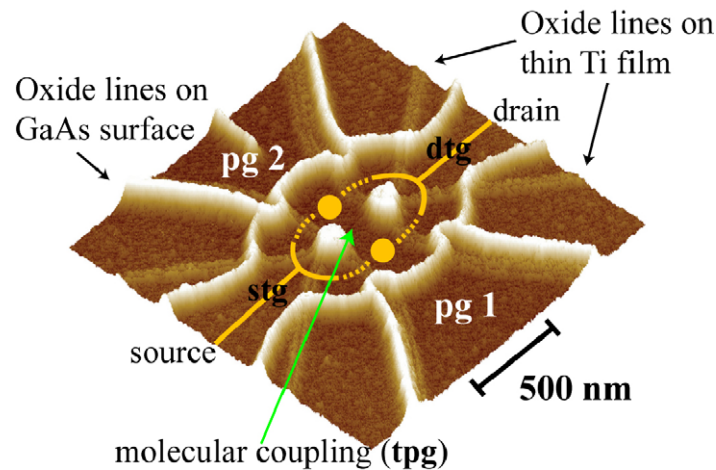
Figure 1. SFM image of the sample surface after multiple layer oxidation. Relevant gate electrodes are labelled. The in-plane gates (white) allow the number of electrons on the two dots to be tuned. Top gate segments (bold black) control the molecular coupling strength and the coupling of the ring to source and drain.

For the fabrication of the nanoscale quantum circuit we use multiple layer oxidation with a scanning force microscope (SFM) [27]. In the first step of this process the surface of the wafer (pre-processed with photolithographic techniques) is locally oxidized following the standard SFM-lithography scheme [28]. At low temperatures the resulting oxide lines on the surface would deplete the underlying electron gas. In the second step, the structure is covered with a 6 nm thick titanium film which is subsequently oxidized locally with the same SFM technique. In this way, a top-gate pattern is created that helps to fine-tune the underlying nanostructure.

The particular sample fabricated for the experiments to be presented is depicted in figure 1. The high and bright oxide lines that can be seen on the sample surface were written on the GaAs surface. They define the ring structure connected to source and drain contacts as indicated in the figure. The two filled circles indicate the location of the two quantum dots, each residing in one interferometer path. Each dot is connected via two quantum point contacts to the ring (dotted lines). Direct molecular coupling between the two dots is possible through an oxide line opening along the direct line connecting the two dots (green arrow). In-plane plunger gate pg1 (pg2) is used for tuning the electron number in dot 1 (dot 2), all other in-plane gates are kept grounded during all experiments.

The titanium top gate is segmented by the faintly visible oxide lines in figure 1. The top plunger gate tpg lies above pg1, but extends over both dots and can therefore be used to control the molecular coupling between the two dots. Two top gate segments with a triangular shape (we denote them with stg and dtg) control the opening of the ring to source and drain.

The experiments were carried out in a dilution refrigerator system at an electronic temperature of 120 mK determined from the width of conductance resonances in the Coulomb blockade regime. A magnetic field can be applied normal to the plane of the electron gas. The differential conductance G has been measured with lock-in techniques with a bandwidth of 0.5 Hz by applying the voltage $+V_{SD}/2$ to the source contact and $-V_{SD}/2$ to drain with $V_{SD} = 12\,\mu\text{Vrms}$ at a frequency below 35 Hz. The alternating current was measured with a homebuilt current-to-voltage converter giving $10^8\,\text{V A}^{-1}$ and having an input noise of $12\,\text{fArms Hz}^{-1/2}$.
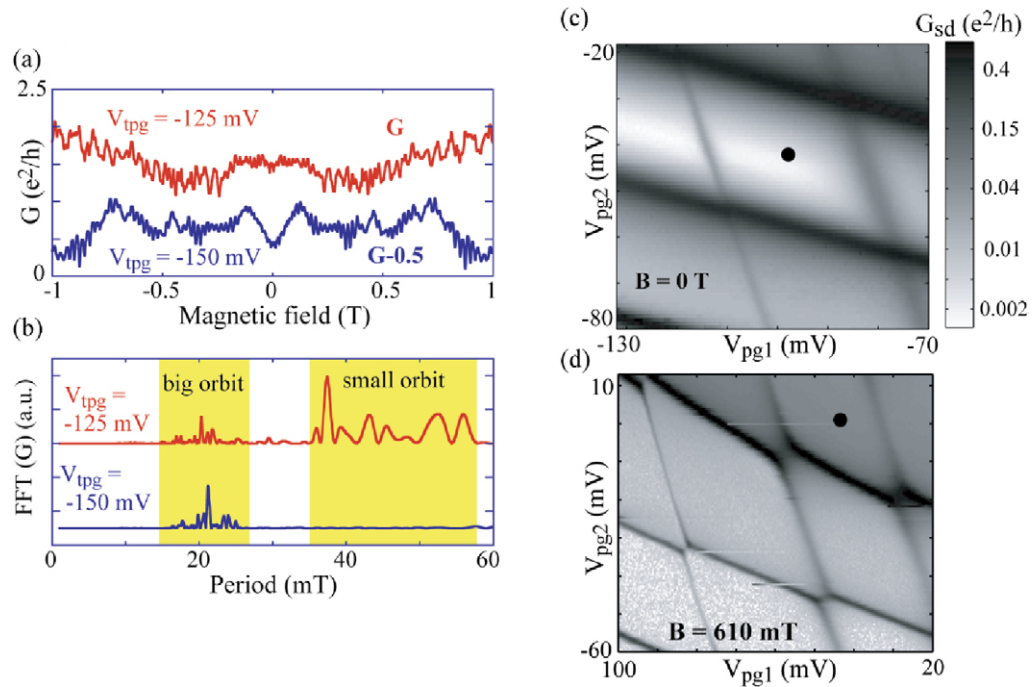
Figure 2. Magnetic field dependent conductance of the interferometer in the open regime for two different values of the top plunger gate. (a) The blue curve shows data for $V_{tpg} = -150$ mV for which the connection between the quantum dot regions is pinched off. The red curve is for $V_{tpg} = -125$ mV where the connection between the quantum dot regions is open. (b) Fourier transform of the data shown in (a). (c) and (d) Differential conductance of the system as a function of the two plunger gate voltages V_{pg1} and V_{pg2}. (c) The direct tunnel coupling between the two dots is completely suppressed. (d) Finite molecular coupling between the two dots is admitted.

3. Sample characterization

In order to characterize the structure, measurements were performed with the quantum dot regions very strongly coupled to the ring, i.e., there is no Coulomb blockade. We determine the properties of the interferometer by measuring the magnetic field dependent G for different voltages V_{tpg} on the top plunger gate tpg. Figure 2(a) shows two example traces. For the blue trace in Figure 2(a) V_{tpg} was set to -150 mV. The conductance shows magnetic field periodic oscillations with dominant periods around 21 mT (see Fourier transform in figure 2(b)). This period corresponds to the 'big orbit' around the entire ring as indicated in figure 1 and we conclude that the direct connection between the two quantum dot regions is depleted at this value of V_{tpg}. From the experimental fact that higher harmonics are not observed we have to conclude that their amplitude is smaller than that of the fundamental period by more than one order of magnitude. In contrast, at $V_{tpg} = -125$ mV (red trace in figure 2(a)), oscillations appear that have a larger periodicity in a magnetic field. The Fourier analysis in figure 2(b) reveals additional contributions from 'small orbits' which make use of the direct connection between the two dot regions, encircle about half the area of the big orbit and have therefore about twice the period.

For a characterization of the quantum dot molecule, we tune the two quantum dots into the Coulomb blockade regime. In previous experiments [24], we have measured the characteristic charging energy of the dots to be 0.7 meV and the characteristic excitation energy to be 0.1 meV. The number of electrons in each dot is of the order of 30. The tunnel coupling of the dots to the ring depends on the exact gate voltage settings, but was lower than the thermal broadening for all experiments. The dots are typically in the single-level tunnelling regime, although accidental level crossings may occur.

When the direct tunnel coupling between the two dots is suppressed by a suitable choice of V_{tpg} (completely dissociated molecule), transport occurs through a parallel connection of the two dots and, neglecting phase-coherent effects, the measured differential conductance is simply the sum of the two individual current paths. The conductance in this situation is depicted in figure 2(c) as a function of the two in-plane gate voltages V_{pg1} and V_{pg2} which tune the electron numbers in the two dots. It shows two sets of parallel conductance resonances, each originating from one of the two dots. It represents the charge stability diagram of the double dot system, meaning that the number of electrons in both dots is fixed and integer in the regions of low current between resonances. If the molecular coupling between the two dots is turned on by increasing V_{tpg} (see figure 2(d)), anticrossings appear and the hexagon pattern characteristic for molecular double dot systems [29] arises.

As a result of the sample characterization we can state that the system represents a fully tunable quantum circuit consisting of a quantum dot molecule embedded in an Aharonov–Bohm interferometer. The molecular coupling and the tunnel coupling of the quantum dots to the ring can be well controlled. The high quality and stability of this structure is a prerequisite for the experiments in [24, 25] and for those presented in the remainder of this paper.

4. Interference: zero-bias phase

We now turn to a set of experiments designed for investigating the evolution of the transmission phase of the quantum dot system in the interferometer. It has been shown in previous experiments [24, 25] that the (elastic cotunnelling) current between resonances of the two quantum dots is partially phase-coherent and Aharonov–Bohm oscillations can be observed. In the following experiments, we will use the electron path through one of the two quantum dots as the reference by keeping the electron number in the respective dot constant. This ensures that the transmission phase through this reference arm does not change significantly. It therefore allows us to investigate the transmission phase through the other arm, where we tune the quantum dot through a number of resonances. However, the measured relative phase is bound to be either 0 (maximum of Aharonov–Bohm oscillations in the conductance at zero magnetic field) or π (minimum of oscillations at zero field) due to the two-terminal nature of our interferometer [11, 12]. Based on general arguments and previous experiments [11, 13] we would expect to see a phase change of π of Aharonov–Bohm oscillations, when a dot goes through a resonance. This corresponds to a change from a conductance minimum to a conductance maximum, or vice versa, at zero magnetic field. Following the notion of the 'universal' appearance of π-phase lapses between neighbouring resonances [13], we would expect to see similar changes in our experiment.

In the simple model introduced in equations (1) and (2) the resonant behaviour of a quantum dot would lead to a resonance in r_1 and to a corresponding phase shift by π in its phase angle δ. Replacing δ in the $\cos \delta$ prefactor of the third term in equation (2) by $\delta + \pi$ leads to a sign change

of this prefactor, i.e., to a change of the zero magnetic field magnetoconductance from minimum to maximum, or vice versa.

4.1. Big orbit

We first show the corresponding measurements in our system with suppressed molecular coupling between the dots. Figure 3(a) shows the corresponding differential conductance as a function of the two in-plane plunger gate voltages V_{pg1} and V_{pg2}. Along the blue (green) trace, the number of electrons in dot 1 (dot 2) is fixed, while that in dot 2 (dot 1) is changed. The double resonance of dot 2 below the starting point of the blue arrow was found to be due to a localized state in the drain contact of dot 2. The strong variations of the charging energy of dot 2 are very likely a result of some states extending further into the drain lead than others.

We investigate the magnetic field dependence of the conductance along the blue and green trace in the plunger gate plane. Figure 3(b) shows the result of the measurement along the green trace, along which six electrons are added to dot 1 while the electron number in dot 2 is constant. In the left panel, raw data are displayed clearly showing the conductance resonances of dot 1. Between the resonances the current is modulated periodically on a scale of 20 mT corresponding to the area of the big orbit. We extract these Aharonov–Bohm oscillations by using a Fourier filter and normalize the amplitude by the magnetic field averaged background conductance (details about this filtering routine can be found in [14], [25]). The resulting data are displayed in figure 3(b) in the right panel. The colour scale has been chosen as to emphasize the periodicity of the oscillations: negative values are plotted in black, positive values in red. Clear oscillations with a relative amplitude of 20% are visible in the regions between conductance resonances. On resonance the Fourier filtering method fails because the resonant peaks shift on fields scales of 100 mT and thereby have a spurious influence on the Fourier spectra. As a consequence, the conductance resonances clearly visible in the left panel appear as smeared stripes in the normalized conductance data of the right panel. In particular in the magnetic field region, say, above 150 mT, the oscillation minima and maxima do not run in parallel to the plunger gate axis. We interpret this behaviour as a changing Aharonov–Bohm period due to a change in the effective area enclosed by the interfering paths. Such a change can arise due to classical Lorentz force effects. Traversing a resonance at constant magnetic field can therefore lead to any apparent phase shift without violating the phase rigidity requirement of the two-terminal device. The latter can only be observed at zero magnetic field.

In figure 3(c), we therefore zoom into the region around zero magnetic field. In particular, we look for changes from maxima to minima (or vice versa) along the $B = 0$ line. In order to facilitate the discussion, conductance valleys between resonances are numbered from bottom to top. Most remarkably, a clear phase change by π is not found for any of the displayed resonances. For example, in conductance valley 1 the observed phase is π (minimum at $B = 0$), in the neighbouring valley 2 it is still π and it remains to be π in valley 3. Close to the resonance between valleys 3 and 4, however, there seems to be a phase change in both valleys giving the sequence π–0–π. Almost in the centre of valley 4, there is a clear phase jump from π to 0 with increasing gate voltage.

We continue the presentation with the data set taken along the blue arrow in figure 3(a) now keeping the electron number in dot 1 fixed and changing the electron number in dot 2 by five electrons. Although the quality of the corresponding data displayed in figure 3(d) is not as high as in figure 3(c), clear Aharonov–Bohm oscillations are visible that reproduce for neighbouring
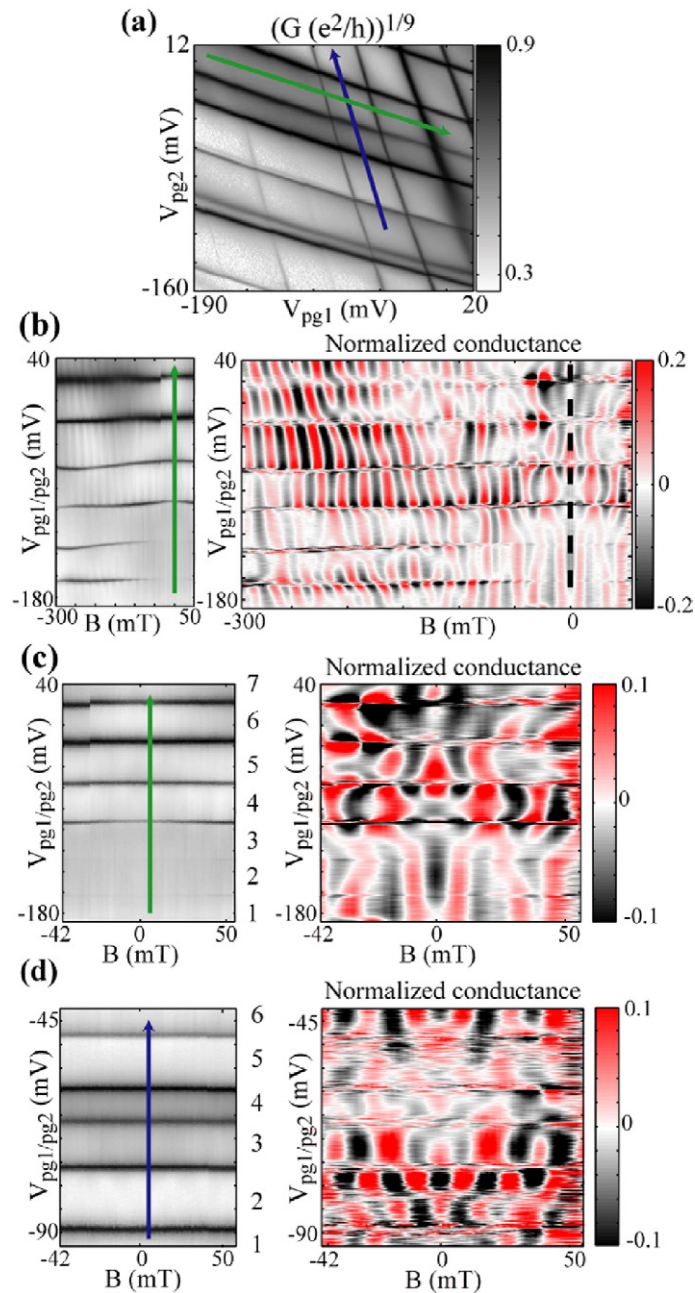
Figure 3. (a) Differential conductance of the system as a function of in-plane gate voltages V_{pg1} and V_{pg2}. Plotting the 9th root of the conductance using a linear colour scale is equivalent to plotting the conductance on a strongly nonlinear colour scale emphasizing the small cotunnelling currents between resonances. (b) Differential conductance measured along the green trace in (a) as a function of the magnetic field. The filtered AB signal is plotted on the right. (c) The conductance (left panel) and filtered data (right panel) is shown around zero magnetic field for the same data as in figure 3(b). Conductance valleys are numbered from bottom to top. (d) The same as (c) measured along the blue arrow in (a).

gate voltage sweeps. In valley 2, we observe a 0–π phase jump with increasing gate voltage. Crossing the resonance between valley 2 and 3, the phase changes from π to 0. The data at higher gate voltages appears to be less reliable, but a 0–π phase jump can be identified traversing the resonance from valley 4 to 5.

Summarizing our findings for the big orbit, we have observed all possible scenarios: crossing resonances may lead to the expected phase jump by π, or it may exhibit no phase jump. In valleys between resonances, we do sometimes observe phase jumps by π, but valleys without such phase lapses exist as well. No 'universal' behaviour is found in our data.

4.2. Small orbit

We have performed further measurements along these lines in a regime of significant molecular coupling between the two quantum dots. This is shown in figure 4(a), where the charge stability diagram consists of the expected hexagon pattern. One connection of dot 1 to the ring was deliberately closed in order to allow only a well defined interference path involving both dots along the small orbit as indicated in the inset. In this configuration, direct sequential tunnelling through dot 2 can be observed. However, direct sequential tunnelling from source to drain through dot 1 is not possible. For example, if a level in dot 1 is in resonance with the Fermi energies in source and drain, but dot 2 is not, an elastic cotunnelling event has to take place transferring the electrons from dot 1 via a virtual state in dot 2 into the drain contact. Dot 2 differs from dot 1 in this configuration, because it is a three terminal quantum dot (see inset in figure 4(a)).

The magnetic field dependence has been investigated along the blue traces a1 . . . f1 and a2 in figure 4(a). Along traces a1 . . . f1, the electron number in dot 2 is kept constant, while it changes for dot 1, and vice versa for trace a2. The corresponding raw conductance data in figure 4(c) taken along trace a2 shows conductance resonances originating from dot 2, while dot 1 is kept off resonance at fixed electron number. Filtering the data as above (figure 3) leads to the plot of normalized conductance shown in figure 4(d). Very clear Aharonov–Bohm oscillations with a period of about 40 mT (small orbit) can be seen. Conductance valleys between resonances are labelled for facilitating the discussion of the data in figures 4(c) and (d). In valleys 1 and 2, the zero magnetic field phase of the oscillations is π (minimum), i.e., it does neither change when the resonance is crossed, nor within the valleys. A π–0–π sequence of phase changes is observed at zero field crossing from valley 2 into valley 3. It seems that the phase of the oscillations on resonance and off resonance differs by π. We show this explicitly by plotting in figure 4(b) the current along the red and blue dashed lines in figure 4(c). The phase difference of π between the two curves is evident.

Figure 4(e) consists of six plots corresponding to the six traces a1 . . . f1 (figure 4(a)). Traces a1 . . . c1 are taken for a fixed number N of electrons in dot 2, but for different position of states relative to the source and drain Fermi energy. Traces d1 . . . f1 are corresponding traces for $N - 1$ electrons in dot 2. Each of the six panels consists of a left and a right part, the left being the raw data (cf figure 4(c)) showing conductance resonances of dot 1, the right being filtered and normalized conductance of the same trace (cf figure 4(d)). All traces have in common that crossing the lowest two resonances of dot 1, the phase at zero magnetic field remains π.

We now focus on the region encircled on all six plots and start the discussion with trace d1. For increasing plunger gate voltages there is a π–0–π–0 sequence of phase changes at zero magnetic field. The two π–0 transitions occur, when a conductance resonance of dot 1 is traversed, while the 0–π transition occurs in the valley between the two conductance peaks. The position in

IOP Institute of Physics ◆ DEUTSCHE PHYSIKALISCHE GESELLSCHAFT
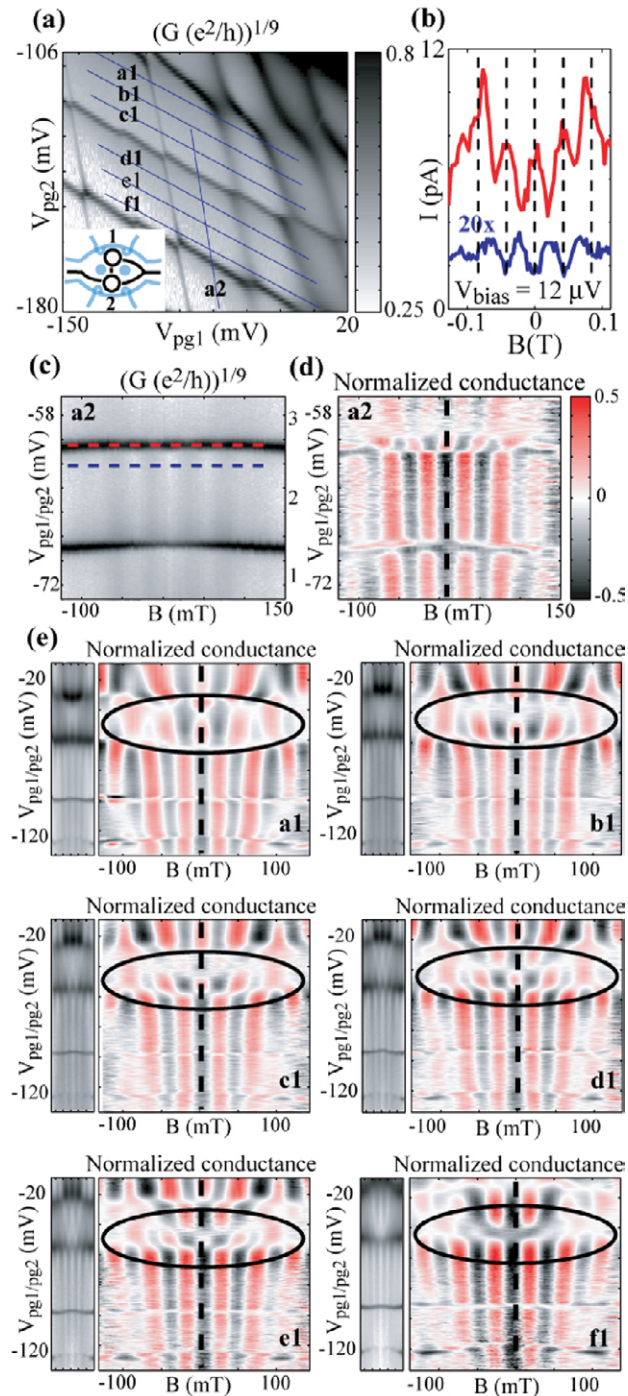
Figure 4. (a) Charge stability diagram of the tunnel-coupled double dot system. Possible interfering paths are schematically illustrated in the inset. (b) Current as a function of magnetic field for dot 2 on resonance (red) and slightly off resonance (blue) as indicated in figure 4(c). (c) The conductance along trace a2 as a function of magnetic field. (d) Filtered data corresponding to figure 4(c). (e) Normalized conductance as a function of magnetic field along traces a1 ... f1. At the left of each panel, the raw data with the conductance resonances of dot 1 are shown.

plunger gate voltage of this latter 0–π transition is shifted down (up) for trace e1 (c1). In traces f1 and b1 this transition has disappeared. In trace a1 it seems that the 0–π transition has cancelled with the π–0 transition that previously occurred on the upper resonance. Correspondingly, in f1 this cancellation occurs at the lower resonance.

A thorough theoretical discussion of the experimental situation described above would require a treatment of the molecular dot–ring system in the cotunnelling regime. Aharonov–Bohm type effects would arise due to the interference of products of four tunnelling matrix elements encountered in tunnelling processes around the small orbit and we expect a rich variety of phenomena to emerge from such a treatment. Our data show again no 'universal' behaviour of the phase: neither the presence or absence of phase changes in conductance valleys nor across resonances seem to follow an obvious rule. The observations emphasize the importance of phase-coherence throughout the whole system and it remains to be theoretically investigated which particular properties of the involved quantum states can be extracted from our measurements.

5. Interference and spin-pairing

It has been proposed in the theory of [26] that the phase-coherent contribution to the current in a system consisting of two quantum dots embedded in a ring should depend on the spin configuration of the two dots. Spin pairing was predicted to lead to a characteristic asymmetry in the visibility of Aharonov–Bohm oscillations in the two tails of a conductance resonance. The effect can be interpreted as being due to spin entanglement in the dots. Recent experiments, where such an asymmetry was observed [22], were interpreted along the lines of this theoretical proposal. In the following, we present results of measurements obtained on our structure.

Crucial for the observation of the effect is the identification of spin pairs, i.e., neighbouring conductance resonances originating from filling the same single-particle orbital with spin-up and spin-down electrons. Previous work [10, 22, 30] has used the following criteria for identifying spin pairs. (i) The magnetic field dependence of spin-pair resonances is similar, both in gate voltage position and in amplitude. (ii) Neighbouring resonances related to different orbital states show a clearly different magnetic field dependence. (iii) The addition energy for the spin-paired electron is smaller than that for the previous or next electron, because there is no confinement energy contribution. These three criteria are not necessarily to be fulfilled in a large magnetic field range starting at zero field, but spin-pairing can arise at finite fields in a limited magnetic field range.

Figure 5 shows a set of measurements made in our sample for interference involving the small orbit. The magnetic field dependent conductance as a function of V_{pg1} is plotted in figure 5(a). Three conductance peaks of dot 1 and Aharonov–Bohm oscillations are observed. We have carefully checked the three above criteria for spin pairing and conclude that peaks 2 and 3 fulfil them, while peak 1 and peak 4 (not on the plot) show a different magnetic field behaviour in the range between 350 and 750 mT. Figure 5(b) shows a zoom into the data of (a) for a smaller magnetic field and gate voltage range. In order to determine the amplitude of the Aharonov–Bohm oscillations normalized to the magnetic field averaged background conductance, we follow a certain oscillation maximum and its neighbouring minimum as a function of magnetic field. The corresponding (B-V_{pg1})-points for the maxima are plotted in blue, the minima in red in the magnetic field–gate voltage plane in figure 5(b). The two resulting curves have naturally a very similar shape, but they have a slight offset in gate voltage due to the
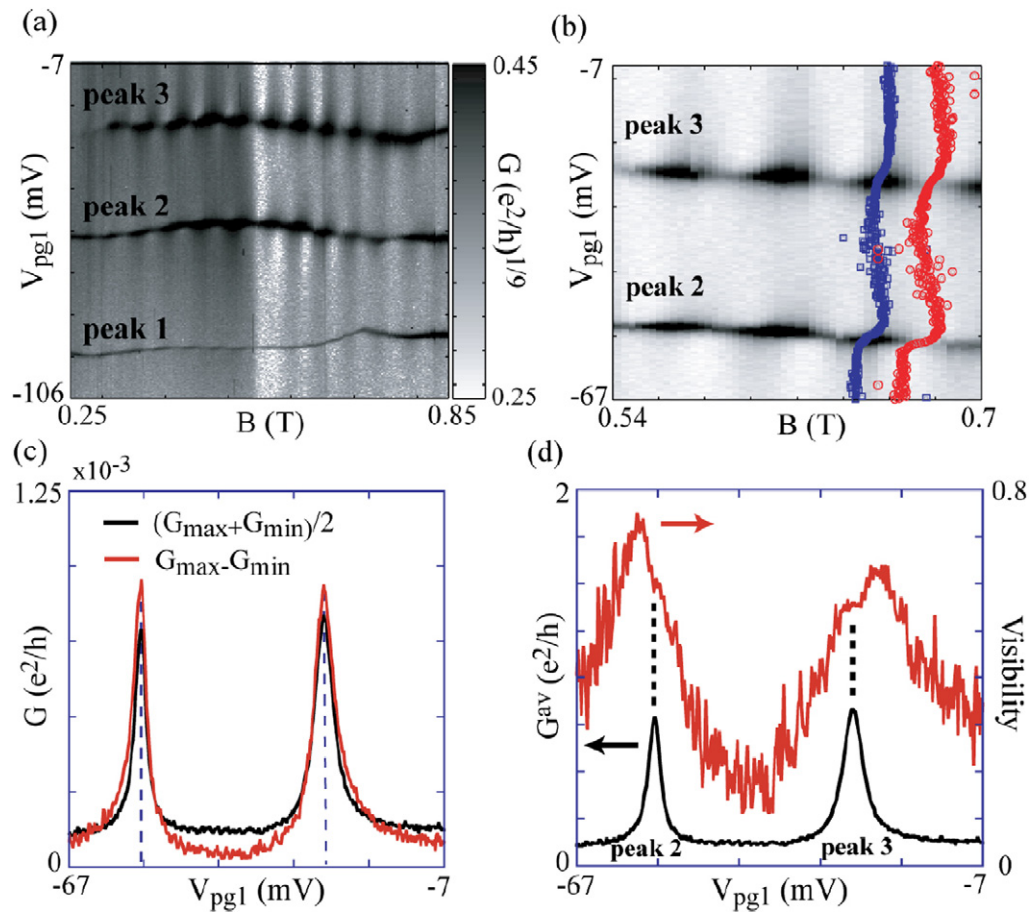
Figure 5. (a) Magnetic field dependent conductance as a function of V_{pg1}. (b) Zoom into (a) showing the two spin-paired peaks and the Aharonov–Bohm oscillations. Blue and red points indicate maxima and minima of the Aharonov–Bohm oscillations (see text for details). (c) Magnetic field averaged conductance (black curve) and Aharonov–Bohm amplitude determined using the neighbouring maximum and minimum marked in (b). (d) Magnetic field averaged conductance (black) and visibility (red) as a function of plunger gate voltage.

shift of the two conductance peaks in magnetic field. We correct for this shift in the calculation of the visibility (v), which is determined from the conductance values at the Aharonov–Bohm maxima (G_{max}) and minima (G_{min}) according to $v = (G_{max} - G_{min})/(G_{max} + G_{min})$. Figure 5(c) shows the magnetic field averaged conductance $(G_{max} + G_{min})/2$ and (twice) the Aharonov–Bohm oscillation amplitude $G_{max} - G_{min}$ as a function of V_{pg1}. While the former shows simply two quite symmetric conductance resonances, the latter quantity exhibits a clear asymmetry. The Aharonov–Bohm oscillation amplitude is larger to the left of the left resonance and to the right of the right resonance than in the conductance valley between the resonances. In the plot of the visibility v in figure 5(d) this asymmetry appears even more pronounced. We have made a similar analysis for a number of other pairs of oscillation minima and maxima in figure 5(b) and consistently found a similarly pronounced asymmetry of the visibility. These results are also similar to those observed in previous measurements [22].

In the simplified coherent single-mode model of equations (1) and (2), the visibility would be given by the expression

$$v = \frac{4\,|r_0|\,|r_1|\,|\cos\delta|}{|r_0|^2 + 2\,|r_1|^2}.$$

In this expression, a symmetric resonant behaviour of r_0 and r_1 cannot lead to an asymmetry in the visibility measured across the resonance. The expected phase change by π in the $\cos\delta$ term leads only to a sign change of the cosine which is not relevant here. Our measured results therefore call for an explanation beyond this simple model. One possibility is the theoretical prediction in [26]. Following the model of these authors, we have to consider the spin of the unpaired electron in dot 1 in the valley between peak 2 and 3. Assuming spin degeneracy of the level, transport can involve a spin flip process in the dot similar to the lowest order contribution to the Kondo effect. Such processes do, however, not contribute to the coherent current, because the tunnelling electron has become entangled with the electron residing in the quantum dot. In contrast, in the valley between peak 1 and 2, there is no unpaired spin in the dot and spin-flip tunnelling is not possible. This asymmetry around peak 2 leads to an asymmetry of the visibility of the Aharonov–Bohm oscillations.

6. Fano effect

The presence of Aharonov–Bohm oscillations demonstrated in all previously discussed measurements of this sample suggests that also the Fano-effect must be observable. It is of particular interest to look for Fano-type of effects in our double dot interferometer geometry, because it has been predicted that the coupling of the two dots via the ring interferometer may lead to unusual interference effects in a single-particle picture [31] and also in the Kondo regime [32]. Among the existing experimental work on the Fano effect in semiconductor nanostructures [17, 18, 20–22], our results are most closely related to [21].

For the purpose of these experiments, the molecular coupling between the two quantum dots was completely suppressed and one interferometer arm was strongly opened (reference arm) such that Coulomb blockade was no longer observed and the transmission was about one mode. As a result there remains only one Coulomb-blockaded quantum dot (the previous dot 2) in the ring. The corresponding conductance in the V_{pg1}–V_{pg2} plane is shown in figure 6(a). The conductance resonances of the Coulomb-blockaded dot 2 can be seen as the steep dark lines running from the top to the bottom of the greyscale plot. Very broad variations of the background conductance originating from the reference arm can be seen in the same figure running parallel to the red line in the figure.

In order to keep the transmission phase in the reference arm constant, magnetic-field dependent measurements were performed along the red line in figure 6(a). The result is shown in figure 6(b). The conductance resonances in dot 2 have only a weak dispersion as a function of magnetic field. Three of the five strong peaks are significantly modulated by the Aharonov–Bohm effect. Figure 6(c) displays cuts of the data in figure 6(b) at constant magnetic field. In particular the two peaks to the left show strongly asymmetric lineshapes characteristic for the Fano effect. The Fano lineshape is changed when the magnetic field is varied, but it is periodic in magnetic field with the Aharonov–Bohm period, as expected. Effects of electrostatic interaction of the dot
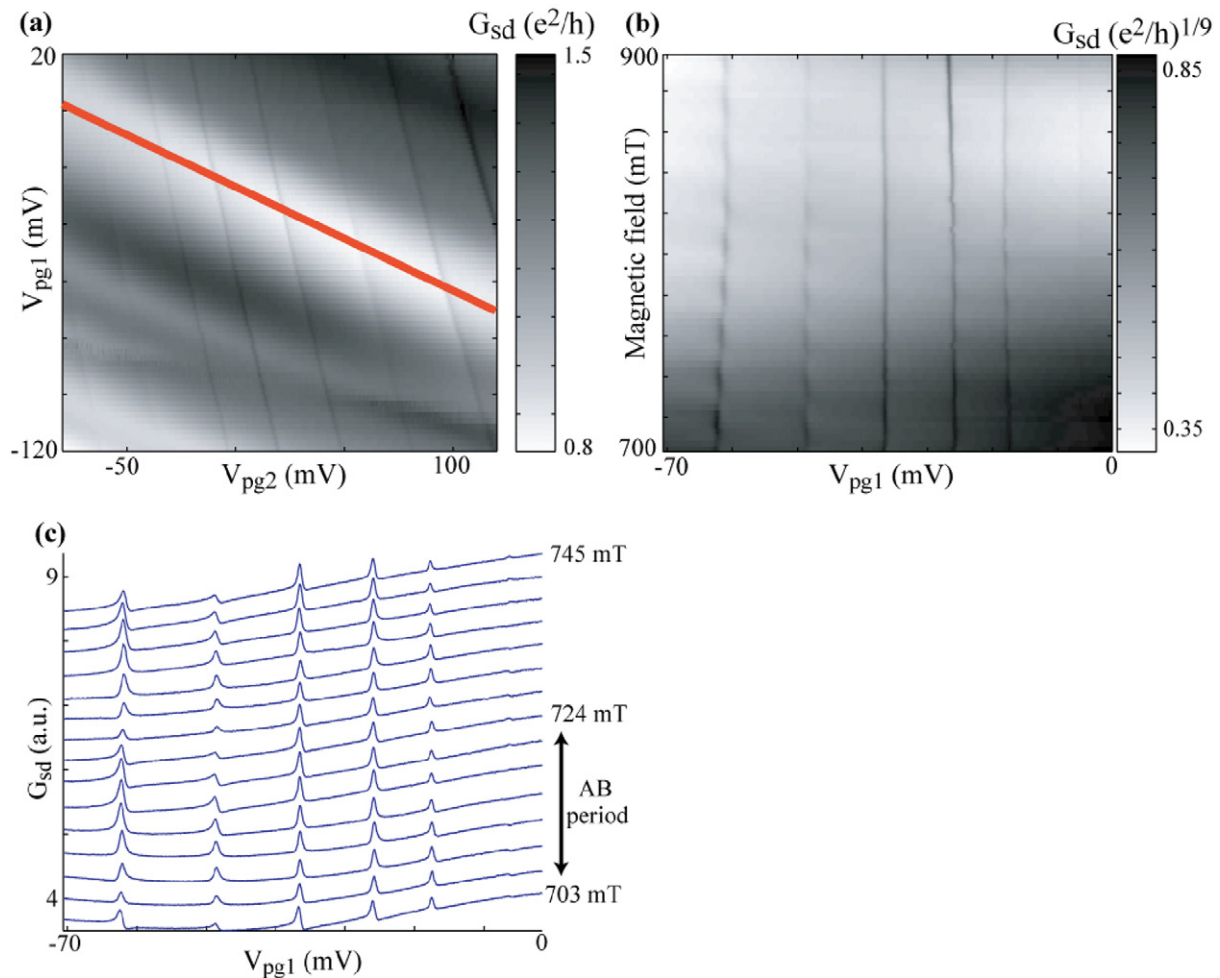
Figure 6. (a) Conductance as a function of V_{pg1} and V_{pg2} with only dot 2 being in the Coulomb blockade region and dot 1 transmitting about one mode. (b) Conductance measured along the red line in (a) as a function of magnetic field and gate voltage. (c) Line traces taken from (b) at constant magnetic field show Fano-type line shapes with a magnetic field periodicity of 22 mT corresponding to the small orbit.

and the reference arm in the spirit of [18] may also be present in the data, but are not further evaluated here.

Instead we briefly discuss attempts to find the unusual interference effects predicted by theory [31, 32] with both dots in the Coulomb blockade. Starting from the above configuration we have tried to tune dot 1 back into the Coulomb-blockade region step by step. However, it turns out that the smaller the transmission through this reference arm becomes, the weaker are the signatures of the Fano-effect, i.e., the asymmetry in the line shapes disappears more and more, and the Aharonov–Bohm effect weakens as well. Further experimental investigations are therefore necessary for the observation of the effects predicted by theory.

7. Triple-dot interference

In this section, we show that the segmented top gates controlling our structure allow to form a coherent triple dot system. Such a triple dot system can be regarded as a further step towards a well controlled quantum circuit. Recently, the stability diagram of a three electron triple dot system has been reported [33, 34]. In the following we demonstrate a well controllable ring-like arrangement of the dots in which phase-coherent coupling can be demonstrated using the Aharonov–Bohm effect. Such an experiment has, to the best of our knowledge, not been reported to date.

For this measurement the top gate stg (see figure 1) was tuned to more negative voltages, eventually driving the opening of the ring to the source contact into the tunnelling regime. The semicircular segment of the interferometer, delimited on one side by the two Coulomb blockaded quantum dots 1 and 2 and on the other side by the tunnel barrier to the source contact thereby forms a third Coulomb-blockaded quantum dot region which we will call dot 3 in the following (see inset of figure 7(a)). The conductance of this triple dot system is shown in figure 7(a) as a function of the two plunger gate voltages V_{pg1} and V_{pg2}. The plot shows a hexagon pattern reminiscent of the double dot system with significant molecular coupling (cf figure 2(d)) with additional resonances running diagonally through the hexagons from the top left to the bottom right. These latter resonances can be assigned to dot 3 for reasons of symmetry because the lever arms of the plunger gates pg1 and pg2 are essentially the same. The resonances of dot 3 show avoided crossings with both resonances of dot 1 and of dot 2 indicating a significant tunnel coupling to both.

In order to demonstrate phase-coherent coupling of this triple dot system we have measured the magnetic field dependent conductance along the yellow trace indicated in figure 7(a). The resulting conductance plotted in figure 7(b) in the left panel shows a number of conductance resonances of all three dots (those that are crossed by the yellow line). Already the raw data exhibits clear Aharonov–Bohm oscillations which can be made even clearer by filtering the raw data. The result shown in the right panel of the figure gives clear evidence for the phase-coherent contribution to the tunnel current through the triple dot system. The Aharonov–Bohm period of about 43 mT is characteristic for the small orbit, as expected.

8. Conclusions

In this paper, we have shown a number of experiments on a quantum dot molecule embedded in a ring interferometer. Excellent stability and full tunability of this structure fabricated with two-layer SFM-lithography turned out to be a key prerequisite for the success of the measurements. The transmission phase of this two-terminal device was measured and the resulting behaviour was neither found to be in obvious relation to simple models nor did it match the 'universal' behaviour observed previously on a multiterminal interferometer. An asymmetric intensity of Aharonov–Bohm oscillations was measured in the region of spin-paired conductance resonances which can be interpreted with recent theories. The structure was tuned into the Fano regime and characteristic asymmetric line shapes were observed exhibiting an Aharonov–Bohm periodicity in a magnetic field. Furthermore, the sample allowed the preparation of a circular triple dot system and the coherent coupling within this system could be demonstrated by the presence of Aharonov–Bohm oscillations. All experiments on this structure demonstrate the feasibility of complex-tailored
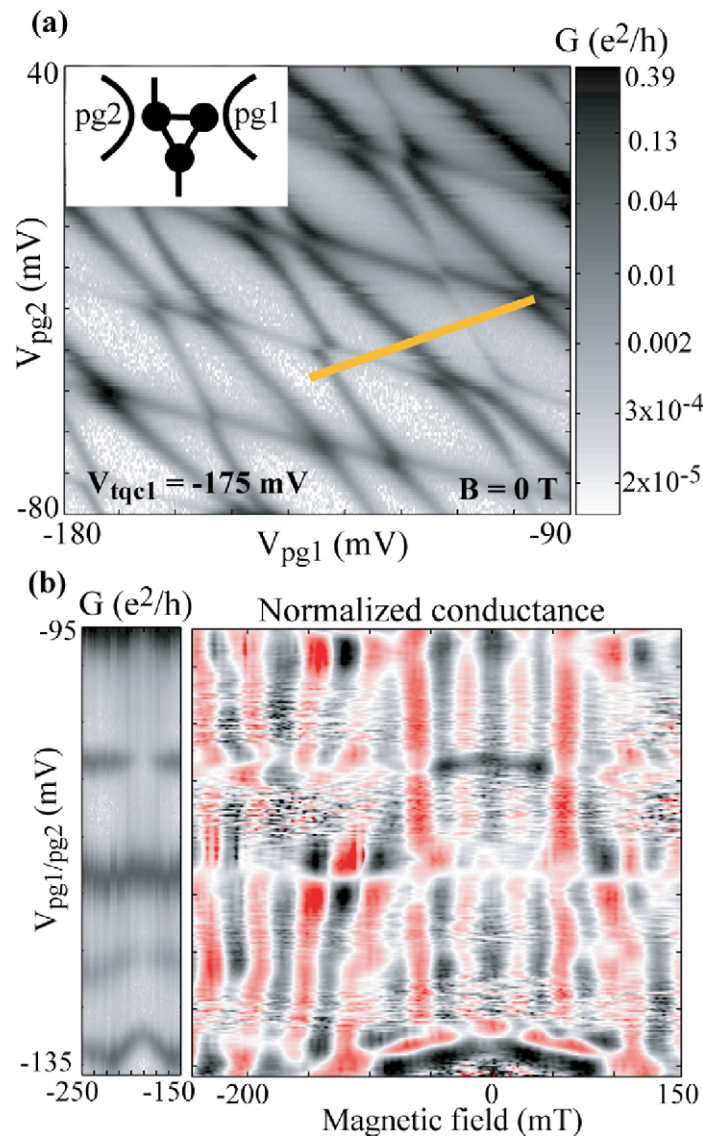
Figure 7. (a) Conductance of the triple dot system as a function of V_{pg1} and V_{pg2}. (b) In the left panel, the raw conductance data are plotted as a function of magnetic field along the yellow line in (a). The filtered data showing clear Aharonov–Bohm oscillations is presented in the right panel.

semiconductor quantum circuits with full tunability and a high degree of phase-coherence as they are anticipated to become important for future technologies in nanoelectronics.

References

[1] Aharonov Y and Bohm D 1959 *Phys. Rev.* **115** 485
[2] Fano U 1935 *Nuovo Cimento* **12** 156
    Fano U 1961 *Phys. Rev.* **124** 1866
[3] Altshuler B L, Aronov A G, Khmelnitskii D E and Larkin A I 1982 *Quantum Theory of Solids Physics Series of Advances in Science and Technology in the USSR)*, ed I M Lifshits (Moscow: MIR) p 130

IOP Institute of Physics Φ DEUTSCHE PHYSIKALISCHE GESELLSCHAFT

[4] Imry Y 2002 *Introduction to Mesoscopic Physics* 2nd edn (Oxford: Oxford University Press)
[5] Washburn S and Webb R A 1986 *Adv. Phys.* **35** 375
[6] Aronov A G and Sharvin Y V 1987 *Rev. Mod. Phys.* **59** 755
[7] Timp G, Chang A M, Cunningham J E, Chang T Y, Mankievich P, Behringer R and Howard R E 1987 *Phys. Rev. Lett.* **58** 2814
       Timp G, Chang A M, DeVegvar P, Howard R E, Behringer R, Cunningham J E and Mankiewich P 1988 *Surf. Sci.* **196** 68
[8] Ishibashi K, Takagaki Y, Gamo K, Namba S, Ishida S, Murase K, Aoyagi Y and Kawabe M 1987 *Solid Sate Commun.* **64** 573
[9] Ford C J B and Ahmed H 1987 *Microelectron. Eng.* **6** 169
[10] Fuhrer A, Lüscher S, Ihn T, Heinzel T, Ensslin K, Wegscheider W and Bichler M 2001 *Nature* **413** 822
[11] Yacoby A, Heiblum M, Mahalu D and Shtrikman H 1995 *Phys. Rev. Lett.* **74** 4047
       Yacoby A, Schuster R and Heiblum M 1996 *Phys. Rev.* B **53** 9583
[12] Büttiker M 1986 *Phys. Rev. Lett.* **57** 1761
[13] Schuster R, Buks E, Heiblum M, Mahalu D, Umansky V and Shtrikman H 1997 *Nature* **385** 417
       Ji Y, Heiblum M, Sprinzak D, Mahalu D and Shtrikman H 2000 *Science* **290** 779
       Ji Y, Heiblum M, Shtrikman H 2002 *Phys. Rev. Lett.* **88** 076601
       Avinun-Kalish M, Heiblum M, Zarchin O, Mahalu D and Umansky V 2005 *Nature* **436** 529
[14] Sigrist M, Fuhrer A, Ihn V, Ensslin K, Ulloa S E, Wegscheider W and Bichler M 2004 *Phys. Rev. Lett.* **93** 66802
[15] McEuen P L, Alphenaar B W, Wheeler R G and Sacks R N 1990 *Surf. Sci.* **229** 312
[16] Lindemann S, Ihn T, Bieri S, Heinzel T, Ensslin K, Hackenbroich G, Maranovski K and Gossard A C 2002 *Phys. Rev.* B **66** 161312
[17] Göres J, Goldhaber-Gordon D, Heemeyer S and Kastner M A 2000 *Phys. Rev.* B **62** 2188
[18] Johnson A C, Marcus C M, Hanson M P and Gossard A C 2004 *Phys. Rev. Lett.* **93** 106803
[19] Kobayashi K, Aikawa H, Sano A, Katsumoto S and Iye Y 2004 *Phys. Rev.* B **70** 035319
       Sato M, Aikawa H, Kobayashi K, Katsumoto S and Iye Y 2005 *Phys. Rev. Lett.* **95** 066801
[20] Fuhrer A, Brunsheim P, Ihn T, Sigrist M, Ensslin K, Wegscheider W and Bichler M 2006 *Phys. Rev.* B **73** 205326
[21] Kobayashi K, Aikawa H, Katsumoto S and Iye Y 2002 *Phys. Rev. Lett.* **88** 256806
       Kobayashi K, Aikawa H, Katsumoto S and Iye Y 2003 *Phys. Rev.* B **68** 235304
[22] Aikawa H, Kobayashi K, Sano A, Katsumoto S and Iye Y 2004 *Phys. Rev. Lett.* **92** 176802
[23] Holleitner A W, Decker C E, Qin H, Eberl K and Blick R H 2001 *Phys. Rev. Lett.* **87** 256802
       Holleitner A W, Blick R H, Hüttel A K, Eberl K and Kotthaus J P 2002 *Science* **297** 70
[24] Sigrist M, Ihn T, Ensslin K, Loss D, Reinwald M and Wegscheider W 2006 *Phys. Rev. Lett.* **96** 036804
[25] Sigrist M, Ihn T, Ensslin K, Reinwald M and Wegscheider W 2007 *Phys. Rev. Lett.* **98** 036805
[26] König J and Gefen Y 2002 *Phys. Rev.* B **65** 045316
[27] Sigrist M, Fuhrer A, Ihn T, Ensslin K, Driscoll D C and Gossard A C 2004 *Appl. Phys. Lett.* **85** 3558
[28] Fuhrer A, Dorn A, Lüscher S, Heinze T, Ensslin K, Wegscheider W and Bichler M 2002 *Superlatt. Microstruct.* **31** 19
[29] Hofmann F, Heinzel T, Wharam D A, Kotthaus J P, Böhm G, Klein W, Tränkle G and Weinmann G 1995 *Phys. Rev.* B **51** 13872
[30] Lüscher S, Heinzel T, Ensslin K, Wegscheider W and Bichler M 2001 *Phys. Rev. Lett.* **86** 2118
[31] Weidenmüller H A 2003 *Phys. Rev.* B **68** 125326
[32] Dias da Silva L G G V, Sandler N P, Ingersent K, Ulloa S E 2006 *Phys. Rev. Lett.* **97** 096603
[33] Vidan A, Westervelt R M, Stopa M, Hanson M, and Gossard A C 2005 *J. Supercond.* **18** 223
[34] Gaudreau L, Studenikin S A, Sachrajda A S, Zawadzki P, Kam A, Lapointe J, Korkusinski M and Hawrylak P 2006 *Phys. Rev. Lett.* **97** 036807